FORCED TO NATURAL CIRCULATION TRANSIENTS IN WIRE-SPACED FUEL PIN BUNDLE

I.Di Piazza[1], R. Marinari[1], D. Martelli[1], M. Tarantino[1]

[1]Italian National Agency for New Technologies, Energy and Sustainable Economic Development, CR. ENEA Brasimone, Italy

Email contact of corresponding author: ivan.dipiazza@enea.it

Abstract

The work reports post-processed data of the experimental campaign carried out in the HLM-operated NACIE-UP facility in the framework of the HORIZON2020 SESAME project. NACIE-UP is a rectangular loop cooled by lead-bismuth eutectic. A prototypical wire-spaced fuel pin bundle simulator (FPS) is installed in the bottom part of the riser, while a shell and tubes heat exchanger (HX) is placed in the upper part of the right descending vertical branch. The difference in height between the heat source (FPS) and heat sink (HX) is about 5.5m and allows the establishment of the natural circulation regime inside the loop. The mass flow rate is measured by a prototypical thermal flow meter. The forced circulation is realized by a gas lift pumping in the riser. Several thermocouples measure temperatures along the loop while the FPS is instrumented with 67 N-type thermocouples.

A PLOFA test is presented in the paper with a power transition from 100 kW to 10 kW and the stop of the pumping gas-lift. Temperature trends showed a coherent behavior with a sharp decrease due to the power decrease followed by local maximum due to the gas-lift stop. The time trend of the main thermal-hydraulic parameters during the transient are illustrated in details. From the experimental data, it is proved that the thermal field develops along the FPS with larger radial thermal differences in top monitored section with respect to the bottom one.

Nusselt numbers in the fully developed top section were computed and exhibited values close to the Kazimi-Carelli correlation. On the initial and final steady states, a statistical analysis was carried out to determine average overall and local values, and the associated uncertainties. The error propagation theory was applied for the derived quantities.

1. INTRODUCTION

The Lead-cooled Fast Reactors (LFRs) are one of the technologies being considered by the Generation IV International Forum (GIF). The adequate physical and thermal properties of the heavy liquid metals (HLMs) increased the interest for their employment as coolant for nuclear systems for the fulfilment of the Generation IV goals [1]. The thermal-hydraulics of HLMs is a relevant aspect for the development of these innovative nuclear systems, being tightly linked to the safety aspects of the reactors. For instance, the study of heat transfer mechanisms in natural circulation regime is outstanding for decay heat removal function in LFRs. Heat transfer mechanism and pressure drop correlations must be evaluated for several kinds of geometries and flow regimes for accurate safety assessment. For this purpose, experimental investigations are more advisable, especially for the evaluation of typical transient behaviours of nuclear interest for the assessment of the coolability of the core during normal and accidental conditions.

The thermal-hydraulics Simulations and Experiments for the Safety Assessment of Metal cooled reactor (SESAME) project was established to deal with thermal-hydraulic issues in support of the development of European liquid metal cooled reactors (ASTRID, ALFRED, MYRRHA, SEALER).

The present paper describes experimental results obtained from the 2017 campaign performed with the NACIE-UP (NAtural CIrculation Experiment- UPgraded) facility, located at ENEA Brasimone Research Centre, in the framework of the SESAME HORIZON2020 project. The designed experiments consist in power or/and mass flow transient which leads to complex transient. These experiments provide system data to qualify STH codes, but also more detailed information on the wire-spaced fuel bundle test section, such as wall temperatures, sub-channel temperatures and heat transfer coefficient (HTC), allowing to test and qualify CFD codes and coupled STH/CFD methods for HLM systems. The old configuration of the facility (NACIE) was already used in the past to verify coupling tools between STH and CFD codes ([2][3][4]).

Concerning the experimental studies on the heat transfer in HLMs-cooled fuel bundle, some works have published in the last years, providing reference data and correlations. For instance, [5] investigated

experimentally the heat transfer and pressure drop in a 19-rod bundle with grid spacer cooled by LBE. They found that measured Nusselt numbers were underestimated by the correlations existing in literature. [6] and [7] measured for the first time the heat transfer coefficient for a 37-pins rod bundle with grid spacers, cooled in a HLM pool. They calculated the Nusselt number as a function of the Péclet number in forced and natural circulation flow, for Péclet numbers in the range 500-3000. [8] assessed the coolability of a wire-spaced fuel bundle cooled by LBE at low and intermediate mass flow rates. The NACIE-UP facility was designed to operate in natural and gas-lift enhanced circulation regimes allowing to cover the low Péclet range of experiments. In fact, similar experiments were carried out at KIT (Germany), focusing on the higher nominal mass flow rates [9].

Most of the studies performed in the past mainly concerned steady state tests, whereas the present work focuses on a PLOFA- like transient, from high power and high mass flow rate to natural circulation at low power. Steady state analysis with uncertainty quantification was also performed for the initial and the final conditions.

2. EXPERIMENTAL SETUP

2.1. NACIE-UP facility

The primary loop of the NACIE-UP facility is shown in Figure 1. It is basically a rectangular loop, where the two vertical pipes, which work as riser and downcomer, are 8 meters long and the two horizontal pipes are 2.4 meters long. The pipes are made in stainless steel (AISI 304) and have a nominal outer diameter (O.D.) 2.5" S40. A prototypical wire-spaced fuel pin bundle simulator (FPS) is installed in the bottom part of the riser, whereas the shell and tubes heat exchanger (HX) is placed in the upper part of the downcomer. The difference in height between the centre of the heating section and the centre of the heat exchanger is about 5.5 m and is essential for the establishment of the natural circulation regime inside the loop. Furthermore, an argon gas injection device is placed inside the riser and, once operating, provides the driving force to enhance the circulation of the primary coolant in the loop. An expansion tank is located at the end of the riser and it is partially filled with argon as cover gas to avoid oxidation and to accommodate the thermal expansion of the LBE. In such configuration, the total LBE inventory of the facility is about 220 l.

The facility includes a secondary system, filled with water at 16 bar, connected to the HX, shell side. It is composed by a pump, a pre-heater, an air-cooler, by-pass and isolation valves, and a pressurizer with argon cover gas. Then, an ancillary gas system ensures a proper cover gas in the expansion tank, provides the gas-lift injection in the riser, and allows the fill and drain system operation. This latter system is composed by ½'' pipes, isolation valves and a storage tank.

The primary loop is instrumented with several bulk thermocouples (TCs) to monitor the fluid temperature along the flow path. In particular TP102, TP103, TP104 are located in the riser, TP310 in the expansion vessel, TP105 in the horizontal upper branch, TP106 and TP107 at the vertical branch downstream the HX, TP101 at the inlet of the FPS. The TCs location can be seen in Figure 2, in the schematic P&ID of the primary system. The mass flow rate of the primary coolant is measured by a prototypical flow meter based on thermal balance (Thermal Flow Meter). This solution was adopted to limit pressure losses in natural circulation conditions. This device is composed by a heating bulb (6 kW maximum), a static mixer and inlet/outlet RTD to measure the temperature difference across the instrument. The error associated to the flow meter is around 5-7%.

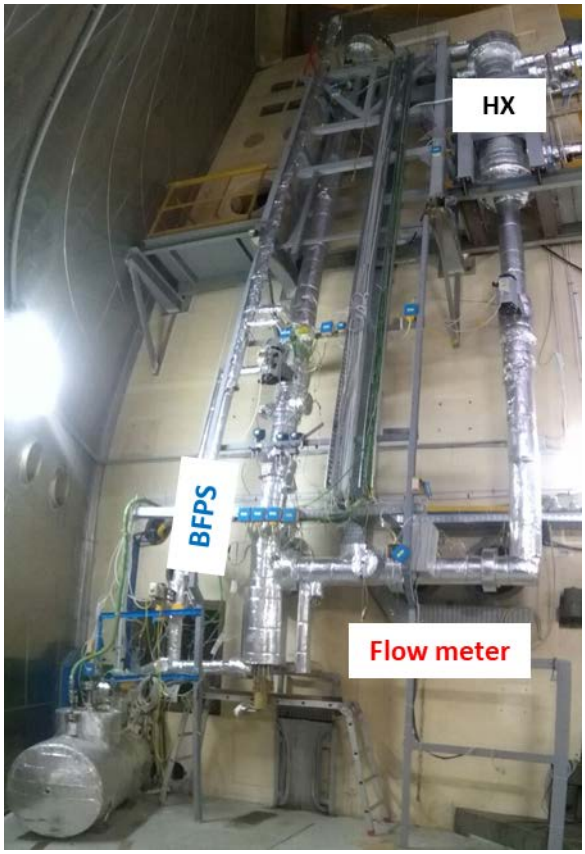

Figure 1 Picture of the NACIE-UP facility primary loop.

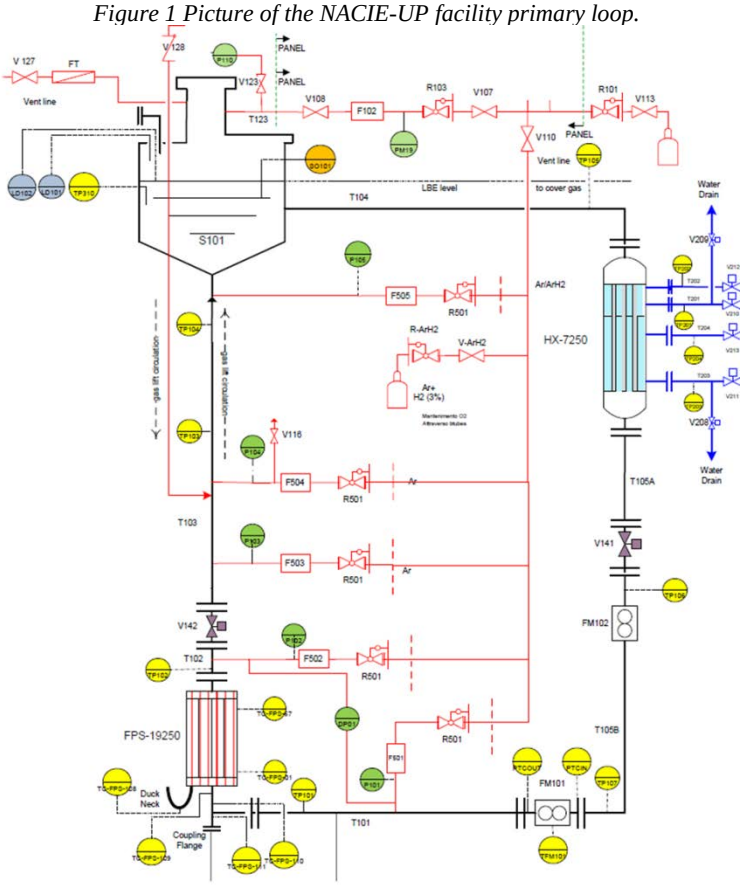

Figure 2 Schematic P&ID of the primary loop with TC locations.

2.2. Gas Injection System

As mentioned in Section 2.1, the facility is equipped with an argon gas injection device, connected to the ancillary gas system. This system ensures a driving force to sustain enhanced circulation regime in the loop and helps to achieve the mass flow rate expected for the test case, in the enhanced circulation regime.

The device currently installed (and used in the tests) for the injection of gas inside the riser is made of a 12.70 mm (1/2 inch) O.D pipe, 6135 mm long, inserted from the 2 ½" coupling flange in the upper part of the expansion tank through a Swagelok tube fitting. The technical drawings of the ending part of the device and its functional dimensions are reported in Figure 9, The gas flows out through five holes (1 mm in diameter) aligned on a generatrix of four short pipes (there are five holes per each pipe). The four short pipes are disposed on a plane perpendicular to the 6135 mm pipe, forming an angle of 90° in relation to each other.

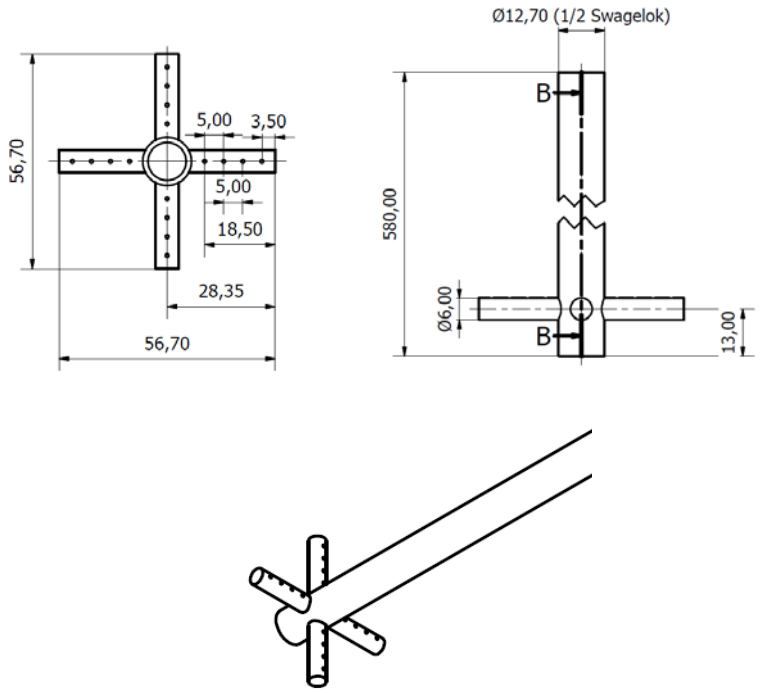

Figure 3 Technical drawings of the gas injection device.

As it regards the gas injection system, the control system allows setting the volumetric flow rate. Nevertheless, it is not possible to know the consequent void fraction α in the NACIE-UP circuit in advance, which would allow to estimate the pressure head provided to the loop. However, it is well known that the relationship between the argon volumetric flow rate and the consequent LBE mass flow rate in the primary circuit is not linear. Further, the gas injection system has some limiting characteristics. The main intrinsic limit and linked to its non-linear behaviour. At high gas mass flow rate, the pumping function saturates, and the system becomes less efficient. The argon in the gas injection system is provided by a compressor that pressurizes a pressure chamber feeding the injector.

2.3. The fuel pin bundle simulator (FPS)

The main test section of the facility is a 19-pins fuel bundle simulator. It is connected to the primary loop of the facility with two 2.5” flanges at the bottom horizontal pipe and in the lower part of the vertical pipe which works as riser. The pins are electrically heated; their overall height is 2000 mm and includes the electrical connectors, a non-active region more than 500 mm long, in order to have a fully developed flow at the inlet of the active zone, which is L_{active} = 600 mm long. A picture of the bundle is shown in Figure 4.

Figure 4: Picture of the Fuel Pin Bundle.

The 19 pins have a diameter D=6.55 mm and are placed on a hexagonal lattice with pitch P=8.4 mm. Wires with a diameter d=1.75 mm are wrapped around the pins with wire pitch P_w=262 mm with the function of spacer. Other main geometrical parameters of the bundle are reported in Table 1. The total flow area can be conventionally divided into 54 sub-channels of three different ranks (S1-S54), as shown in the schematic sketch of the cross section of the bundle in Figure 5. The central rank is represented by the central pin 1 and by sub-channels S1-S6; the middle rank is represented by pins 2-7 and by sub-channels S7-S24; the external rank is represented by the pins 8-19 and by sub-channels S25-S54. Nevertheless, the hydraulic diameter of the equivalent infinite lattice of rods, $D_{H,nom}$, is used to define the non-dimensional quantities in the post-processing of the results.

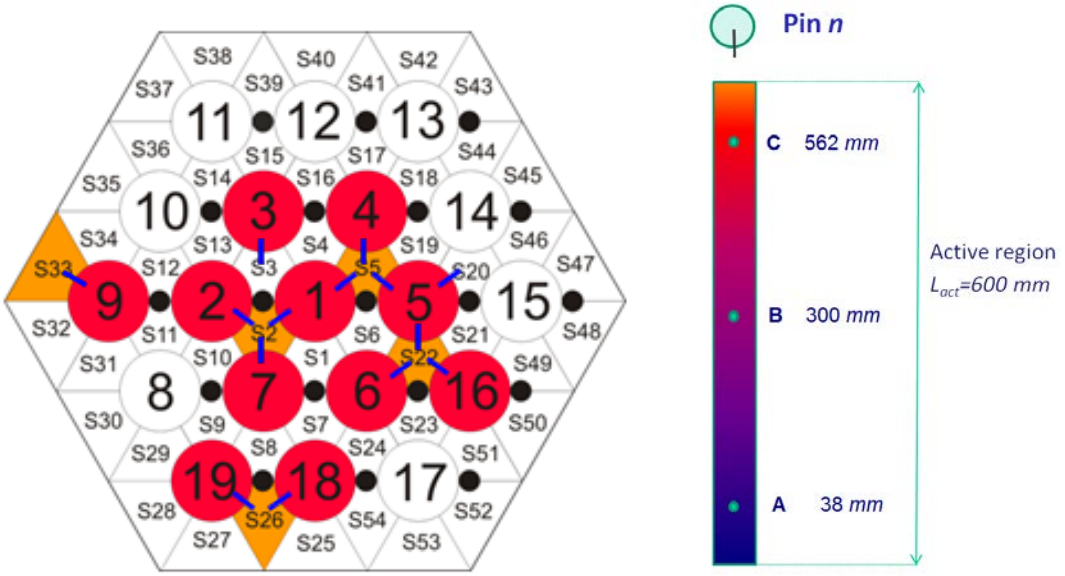

Figure 5: Axial position (left) and sketch of the monitored sections (right) of the fuel pin bundle simulator. Instrumented pins in red; instrumented sub-channels in orange, wires in black and wall TCs position in blue.

Table 1: Fuel pin simulator (FPS) main dimensions.

Dimension	Symbol	Value
Number of pins	M	19
Pin outer diameter	D	6.55 *mm*
Pitch	P	8.4 *mm*
Pitch-to-diameter ratio	P/D	1.2824
Wire diameter	d	1.75 *mm*
Wire pitch	P_w	262 *mm*
Total length	L_{tot}	2000 *mm*
Active length	L_{active}	600 *mm*
Total flow area	A	65.49 mm^2
Hydraulic diameter of the bundle	$D_{H,bdl}$	4.147 *mm*
Hydraulic diameter of the equivalent infinite lattice	$D_{H,nom}$	3.836 *mm*
Hexagonal wrapper apothem	a	19.67 *mm*

Instrumented pins are depicted in red and the monitored sub-channels are in orange in Figure 5. Three different axial positions are instrumented: z= 38, 300, and 562 mm after the beginning of the active region, named section *A*, *B* and *C*. It should be mentioned that the three axial positions are exactly in the same configuration, being the wire pitch P_w=262 mm= 300-38 mm= 562-300 mm. This choice allows having three measurements of heat transfer referred to the same relative position of wire and pins. Pins 2, 4, 6, 7, 9, 16, 18, 19 are equipped with wall embedded thermocouples (0.35 mm thick) on generatrixes parallel to the pin axis. Further, pin number 3 is instrumented along a generatrix with 13 wall embedded thermocouples along the active length, placed every P_w/6=43.66 mm starting from section A. The total number of wall embedded thermocouples is 52. At each measurement section, wall embedded TCs move azimuthally around the pin to reach the correct azimuthal position, which is depicted in blue in Figure 5. The wall TCs are placed inside the clad, in a groove 0.38 mm thick. It is considered that the thermocouple measures the temperature at the junction (located at the centre) so a correction is needed to evaluate the temperature at the clad outer surface. Further, sub-channels S2, S5, S22, S26, S33 are instrumented with bulk thermocouples 0.5 mm thick, at the same three measurement sections z=38, 300, 562 mm, for a total number of 15 bulk thermocouples. The bulk thermocouples run following the wire associated to the pin closest to the monitored sub-channel (e.g. pin 1 for sub-channel S5). The hot junction is placed in the centre of the monitored sub-channel and the TC wire is prolonged to form an arc to increase its mechanical stiffness, aiming to guarantee the correct position when exposed to the LBE stream. The TC head is fixed to the spacing wire by point welding. All the thermocouples adopted in the FPS are 'K' type with a certified accuracy of 1.5 *K*.

2.4. Thermal flow meter

A prototypical thermal flow meter (FM101) was used to measure the LBE mass flow rate in the loop. The thermal flow meter is based on the energy balance and it is shown schematically in Figure 6.

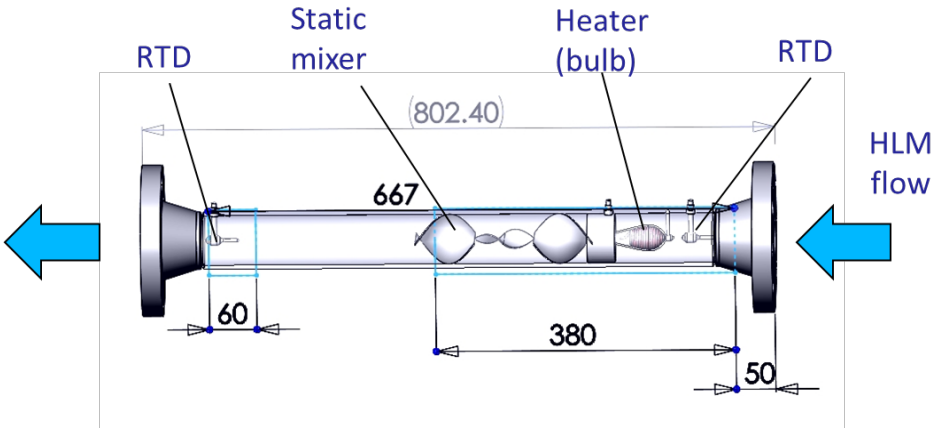

Figure 6 Schematic view of the thermal flow meter.

The component is made by a flanged pipe (SS) with an heater developed by Thermocoax (6 kW maximum power), a static mixer, 2 Resistance Temperature Detector (RTD) and an internal RTD in the bulb. The mass flow rate will be computed by the thermal balance:

$$\dot{m} = \frac{Q_{tfm}}{c_p \cdot \left(T_{out} - T_{in}\right)} \tag{1}$$

In stationary conditions, Eq. (1) provides the correct value of the mass flow rate. In transient conditions, the bulb heater is properly regulated to guarantee that the temperature difference between the bulb heater and the inlet RTD remains constant. Moreover an inlet-outlet temperature compensation is adopted to keep into account the travelling time of the fluid through the 800 mm pipe. These two latter implementations in the Data and Acquisition Control System (DACS) of the instrument provide fast and accurate response to transients.

The thermal flow meter was developed in ENEA in collaboration with Thermocoax and it was successfully tested first in water and then in HLM in several experimental campaign in NACIE facility. With respect to other technologies, it has the advantage to have very low pressure losses and a very high limiting working temperature. It is accurate even at low flow rates in HLM down to 0.6 kg/s. The thermal flow meter with 'thermal balance' showed good features in stability and repeatability, good response to transients and no need of calibration because it is based on basic conservation laws.

For the NACIE-UP facility in this configuration, the thermal flow meter FM101 is set to measure flow rates going from 0.6 kg/s to 10 kg/s. The correspondence between the electrical signal (current) and measured flow rate is 4-20 mA →0.6-10 kg/s. The accuracy was evaluated by the error propagation theory and it is around 11%.

3. EXPERIMENTAL CONDITIONS

The experimental campaign designed in the framework of the SESAME project focused on three fundamental tests concerning power and/or gas lift transition and was intended to analyse the thermal-hydraulic behaviour of the fuel assembly cooled by heavy liquid metal during a Loss of Flow Accident (LOFA)-like transient.

The first two test consisted in a gas transition at constant power and power transition with constant argon flow rate and are not reported in this paper.

The third fundamental test consisted in a power and mass flow rate transition, starting from a steady state condition characterized by high power and high mass flow rate and getting to low power with low mass flow rate in natural circulation flow. The starting steady state condition was characterized by a total power in the FPS of 100 kW and a gas flow rate equal to 20 Nl/min. The transition consisted in the decrease of the FPS power to 10 kW with a power rate equal to 10 kW/s and the gas injection device was switched off, taking about 1 second to decrease to zero. After the transition, a new steady state condition was awaited and maintained for additional time.

For all the experimental tests, the secondary side was filled with water at 16 bar and operated with an inlet HX temperature of 170 °C and a total volumetric flow rate of 10 m^3/h, using just the high power section of the heat exchanger. These condition are kept constant and a PID regulates the secondary water inlet temperature by a secondary on-line heater.

Only the results from the third fundamental test (PLOFA transition) will be reported in detail, being the most complete test.

4. POST-PROCESSING METHODS

4.5. Definitions and derived quantities

The instrumentation in the NACIE-UP facility allowed to obtain direct measurement of the nominal power, of LBE mass flow rate, of the LBE temperatures in the loop and localized wall and sub-channel temperatures in the bundle. The section-averaged temperature inside the bundle was estimated from the measured sub-channel temperatures.

The wall temperatures are measured by embedded thermocouples which are placed inside the clad, in a groove 0.38 mm deep. This mounting system does not modify the geometry of the pin, which remains cylindrical and the fluid flow and heat transfer in the sub-channel are not perturbed. However, wall embedded TCs measure a temperature in a position slightly inside the clad, higher than at the clad outer surface. A correction for this effect was implemented by applying the heat conduction law in cylindrical geometry.

The nominal power is directly measured by the DACS, whereas the effective power released in the active length was estimated through an energy balance, following Eq. (2):

$$Q_{eff} = \dot{m} \cdot \overline{c}_p \cdot (T_{out} - T_{in}) \tag{2}$$

where $\overline{c}_p$ is the LBE specific heat at average temperature between FPS inlet (T_{in}) and outlet (T_{out}). It resulted that the effective power Q_{eff}, released in the active region, is about 90% of the nominal power Q_{nom}. The remaining 10% of the power is released outside the active region due to losses in the cold tails and in the non-active part. This estimation derived from post-processing of experimental data in different test conditions. This quantity can be estimated following the calculation of Q_{pre}, in Eq. (3):

$$Q_{pre} = \dot{m} \cdot \overline{c}_p \cdot (T_{in} - TP_{101}) \tag{3}$$

where $\overline{c}_p$ is now the LBE specific heat at average temperature between TP101 and FPS inlet (T_{in}).

For post-processing analysis, some non-dimensional numbers are used. Reynolds number, Péclet number and Nusselt number were properly defined.

4.6. LBE physical properties

In the present work, LBE physical properties, which are all temperature-dependent, are evaluated using empirical correlations suggested in the OECD/NEA Handbook (Nuclear Energy Agency, 2015). Formulas for density, specific heat, dynamic viscosity, conductivity are reported in Table 2. The maximum deviation of the experimental data with respect to the correlation is also reported. The standard deviation of the experimental

data with respect to the related correlation was computed from the source data reported in the OECD/NEA Handbook for each physical property and it is reported in the last column.

Table 2: Physical properties of LBE as a function of temperature (T in Kelvin), from LBE-Handbook [3].

Property	**Symbol**	**Correlation**	**Maximum Uncertainty**	**Standard deviation**
Density	$\rho(\mathrm{T})$	$11065 - 1.293 \cdot T$	$\leq 0.8\%$	0.58%
Heat capacity	$c_p(T)$	$164.8 - 3.94 \cdot 10^{-2} \cdot T + 1.25 \cdot 10^{-5} \cdot T^2 - 4.56 \cdot 10^{-5} \cdot T^{-2}$	$\leq 5.0\%$	2.4%
Dynamic viscosity	$\mu(\mathrm{T})$	$4.94 \cdot 10^{-4} \exp\left(\frac{754.1}{T}\right)$	$\leq 6.0\% - 8.0\%$	7.2%
Thermal conductivity	$k(T)$	$3.284 + 1.67 \cdot 10^{-2} \cdot T - 2.305 \cdot 10^{-6} T^2$	$\leq 10.0\% - 15.0\%$	6.2%

4.7. Uncertainty analysis

Several sources of uncertainties need to be taken into account in analyzing the experimental data. For each raw measured quantity X, two sources of error must be considered, i.e. the sampling statistical error and intrinsic instrumental error. The total uncertainties for each acquired variable is computed as in Eq. (4).

$$\sigma_{Xi,tot}^2 = \sigma_{Xi,stat}^2 + \sigma_{Xi,instr}^2 \tag{4}$$

Another source of error to be considered is the uncertainty on the LBE physical properties, and the value indicated in the last column of Table 2 are used for this purpose.

Following the error propagation theory, the uncertainties of a derived quantity *Y*, which is function of *n* variables X_i (see Eq. (4)), is computed from the standard deviation of the *n* variables, following Eq. (6).

$$Y = f\left(X_1, ..., X_n\right) \tag{5}$$

$$\sigma_Y^2 = \sum_{i=1}^{n} \left(\frac{\partial f}{\partial Xi} \cdot \sigma_{Xi} \right)^2 \tag{6}$$

5. EXPERIMENTAL RESULTS OF FUNDAMENTAL TEST III

The fundamental test 3 consisted in both FPS power and gas-lift transition. The nominal FPS power was initially set at 100 kW and decreased to 10 kW at time t = 1335 s from the beginning of the transient. The power decrease was set to be 10 kW/s, so the nominal power stabilized at 10 kW at about time 1345 s (10 s later). Figure 7 *(a)* shows the time trend of the nominal power and the actual power released along the active length of the FPS in fundamental test 3, and Figure 7 *(b)* illustrates a detail of the FPS power at the beginning of the transient. The nominal gas flow rate was initially set at 20Nl/min and then it was switched off. The decrease of gas flow rate was triggered after that the power transition was completed, in order to avoid high peak clad temperatures and to preserve the bundle integrity (Protected loss of flow). The resulting experimental trend of the Ar flow rate is reported in Figure 8. The decrease of the gas flow from 20 Nl/min to 0 Nl/min lasted about 1 s.

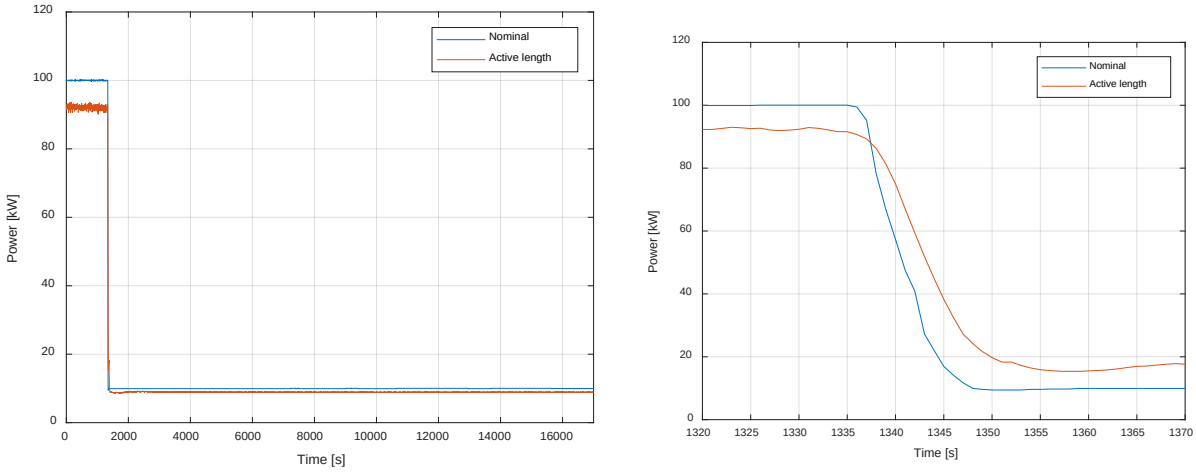

a) *b)*

Figure 7: Time trend of the FPS power (a) and zoom of the transition (b), fundamental test 3.

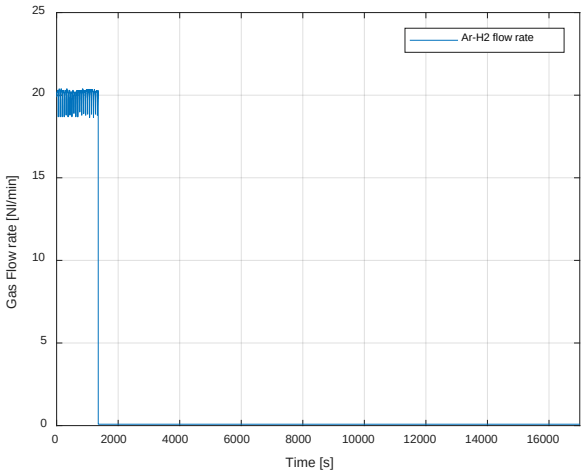

Figure 8: Time trend of the gas flow rate during fundamental test 3.

Figure 9 shows the time trend of the LBE mass flow rate obtained during the test in the loop. After the power and gas transition, the LBE mass flow rate decreased sharply; then there is a local relative maximum followed by a smooth decrease. The time trend of the LBE temperature inside the main loop is illustrated in Figure 10. The water temperature at the inlet of the HX (TP208) was set to 170°C and the DACS regulates the secondary side pre-heater in order to obtain the desired value. The oscillation of the control system are small and therefore the value can be considered approximately constant.

The coldest part of the loop is the lower part, situated between the HX outlet and the flow meter inlet (TP106 and TFM-In), the temperature increases few °C (TFM-Out and TP101) inside the thermal flow meter due to the power released from the instrument. The hottest part of the loop is downstream the FPS (TP102), in the riser (TP104) and in the upper part of the loop (TP310 and TP105). When the FPS power was decreased from nominal 100 kW to nominal 10 kW, TP102 suddenly decreased and the other parts of the loop followed. However, the decrease of the temperatures in TP310 and TP105 is lower and reflects the time needed to replace the LBE inventory in the expansion vessel capacity. When the gas was switched off, the LBE mass flow rate suddenly decreased and it caused a small peak in the LBE temperature at the thermal flow meter outlet, which can be noticed in TFM-Out, TP101 measurements in Figure 10. This local peak was due to the presence of the thermal mass flow meter in the cold leg, which releases a certain amount of power for its operation.

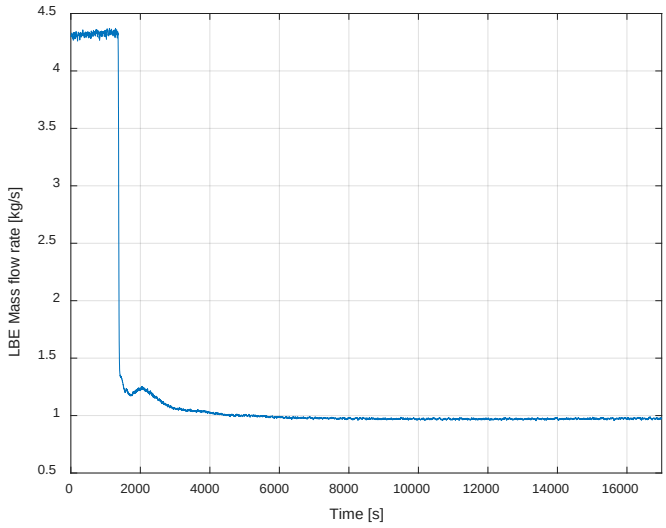

Figure 9: Time trend of the LBE mass flow rate during fundamental test 3.

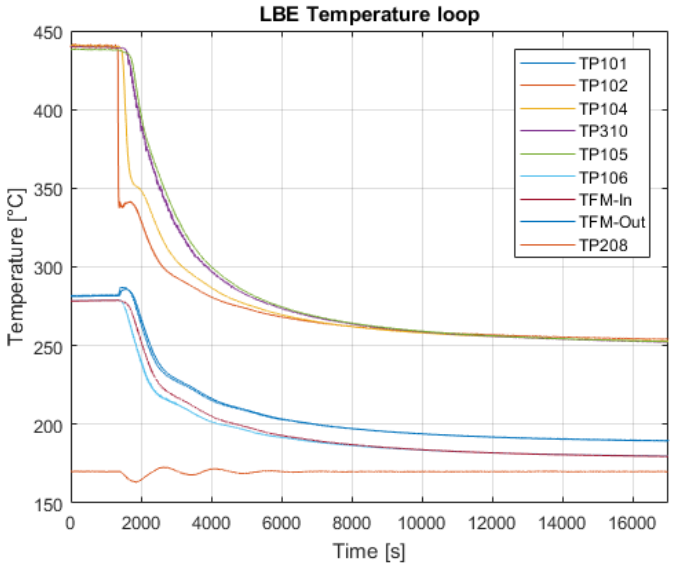

Figure 10: LBE temperature inside the NACIE-UP loop, fundamental test 3.

The section-averaged LBE temperature at the inlet, at the outlet of the active region of the bundle and at the three monitored sections is shown in Figure 11. The LBE temperature inside the FPS decreased in accordance with the reduction of the FPS power, then a peak in all the temperatures occurred when the gas flow rate was switched off. This peak is due to the onset of the natural circulation with a minimum in the LBE mass flow rate. After the transition the LBE temperatures stabilized to new lower values. The new steady state was reached after several hours. Figure 12 illustrates the LBE temperature in the monitored sub-channels S2 (central subchannel) and S22 (peripheral subchannel). The temperature difference between the two sub-channels, at each section, decreased from the first to the second steady due to the reduction of the power generated inside the pins. Moreover, the temperature difference between central subchannel (S2) and peripheral subchannel (S22) increased going from section A to section C; this is due to the fact that thermal fields develops along the heated length; this remarkable result is found experimentally. Moreover, the behaviour can be observed both in the stationary state and during the transition from forced to natural circulation.

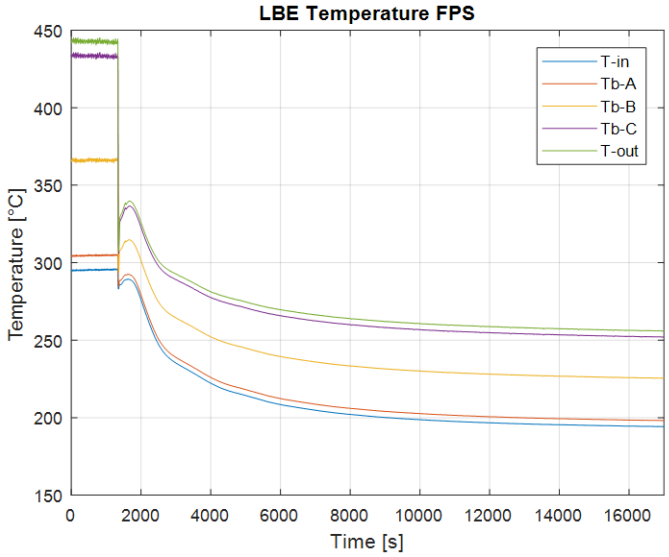

Figure 11: LBE average temperature inside the FPS, fundamental test 3.

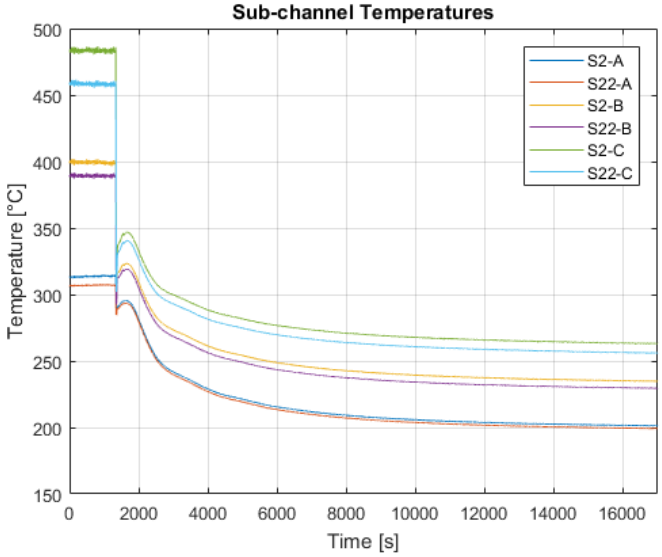

Figure 12: LBE temperatures in sub-channels S2 and S22, at the three monitored sections (A, B, C), fundamental test 3.

Experimental transients were repeated two times and similar results were obtained in both cases: data repeatability was therefore proved.

5.8. Steady state analysis

For further analysis, the average Nu versus Pe from all the three fundamental tests is reported in Figure 13. The values were obtained at the initial and final steady states of the test and were reported with their error bars on the x and y coordinates. The two already mentioned correlations of Kazimi-Carelli [11] and Ushakov [12], as well as a third correlation from literature suggested by Mikityuk [13], were also reported as reference. The general trend is in accordance with Kazimi-Carelli correlation for the more developed sections B and C. Section A shows coherently higher values, since it is located at the beginning of the active region and the temperature difference between the wall and the LBE is relatively small because the thermal boundary layer is

not developed. According to these results, the Kazimi-Carelli correlation seems to be more in accordance with experimental data and should be used for predictions in wire spaced HLM bundles with P/D around 1.28.

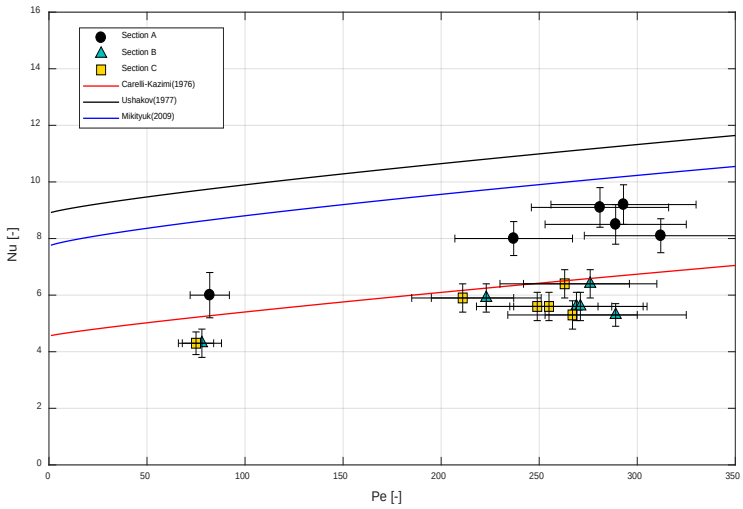

Figure 13: Section-averaged Nusselt number versus Péclet at steady state, for the three Fundamental Tests.

6. CONCLUSIONS

This paper describes the main outcomes of the experimental campaign performed in the NACIE-UP facility at ENEA Brasimone R.C. for the SESAME EU project.

The three fundamental tests concerned transients respectively with gas lift transition, power transition and the combination of the two (power and gas reduction, Protected Loss of Flow Accident, PLOFA) and focus on the study of the thermal-hydraulic behaviour of the loop and the bundle during power and mass flow transient. Only the third test (PLOFA) was presented in detail in this work. The loop is instrumented with several thermocouples both to monitor temperatures in the flow path and inside the fuel pin simulator test section, which consists in a 19-pins wire-spaced bundle with a geometry representative of the MYRRHA fuel assembly.

Mass flow rate and temperature in the loop were reported and discussed. Mass flow rate was measured by a prototypical thermal flow meter. Temperatures showed a sharp decrease in the transition followed by a local maximum and a final steady state with values lower than the initial steady state. Further, the analysis of the initial and final steady states was performed with uncertainty analysis. The main system parameters, as well as non-dimensional numbers in the bundle (at the three monitored sections), were computed and analysed for the stationary conditions. From the data analysis, it emerges that the FPS power is not released entirely in the active region, but a part of the power (between 8-10 %) is released in the zone upstream the active one (600 mm long).

A summarizing graph, displaying the trend of the average Nusselt as function of the average Péclet number, shows that most of experimental data follow a similar trend with respect the Kazimi-Carelli correlation available in literature. This result is consistent with previous experimental campaigns with the same test section [8] and it was expected. A strong subchannel rank effect emerges from the experimental data, with the central subchannels hotter than the peripherals ones. As it was expected, the temperature difference increases going from section A to section C due to the developing thermal conditions. Lots of data, both integral and local, were produced and published; the aim is that this information can be used to qualify STH codes, verify CFD codes and coupled STH/CFD methods for HLM systems.

ACKNOWLEDGEMENTS

This work was performed in the framework of the H2020 SESAME project. This project has received funding from the Euratom research and training program 2014-2018 under grant agreement No 654935.The work described in this paper was funded also by the Italian Minister for Economic Development (MiSE) in the frame of the FRAMEWORK AGREEMENT (ADP) MiSE-ENEA (2010-2018). The views and opinions expressed herein do not necessarily reflect those of the European Commission or the Italian Government.

The authors wish to acknowledge the input and contributions of all international colleagues involved. The authors wish to thank all the ENEA's technicians involved in the implementation and operation of the LFR R&D program.

REFERENCES

[1] Generation IV International Forum, 2014, January, Technology Roadmap Update for Generation IV Nuclear Energy Systems.

[2] Martelli, D., Forgione, N., Barone, G., Del Nevo, A., Di Piazza, I., Tarantino, M., "Coupled simulation of natural and forced Circulation Tests in Nacie Facility Using Relap5 and Ansys Fluent Codes", Proceedings of International Conference On Nuclear Engineering, ICONE22, Prague 2014, pp. 1–10.

[3] Martelli, D., Forgione, N., Barone, G., Di Piazza, I., Coupled simulations of the NACIE facility using RELAP5 and ANSYS FLUENT codes, Annals of Nuclear Energy 101 (2016) 408-418.

[4] Angelucci, M., Martelli, D., Barone, G., Forgione, N., Di Piazza, I., STH-CFD codes coupled calculations applied to HLM loop and pool systems, Science and Technology of Nuclear Installations 201 (2017) Article ID 1936894, 13 pages.

[5] Pacio, J., Daubner, M., Fellmoser, F., Litfin, K., Marocco, L., Stieglitz, R., Taufall, S., Wetzel, Th., Heavy-liquid metal heat transfer experiment in a 19-rod bundle with grid spacer, Nucl. Eng. Des. 27 (2014) 33-46.

[6] Martelli, D., Forgione, N., Di Piazza, I., Tarantino, M., HLM fuel pin bundle experiments in the CIRCE pool facility, Nucl. Eng. Des. 292 (2015) 76-86.

[7] Tarantino, M., Martelli, D., Barone, G., Di Piazza, I., Mixed convection and stratification phenomena in a heavy liquid metal pool, Nucl. Eng. Des. 286 (2015) 261-277.

[8] Di Piazza, I., Angelucci, M., Marinari, R., Tarantino, M., Forgione, N., Heat transfer on HLM cooled wire-spaced fuel pin bundle simulator in the NACIE-UP facility, Nucl. Eng. Des. 300 (2016) 256–267.

[9] Pacio, J., Daubner, M., Fellmoser, F., Litfin, K, Wetzel, T., Experimental study of heavy-liquid metal (LBE) flow and heat transfer along a hexagonal 19-rod bundle with wire spacers, Nucl. Eng. Des. 301 (2016) 111–127.

[10] Nuclear Energy Agency, 2015. Handbook on Lead-bismuth Eutectic Alloy and Lead Properties, Materials Compatibility, Thermal-hydraulics and Technologies, OECD/NEA.

[11] Kazimi, M.S., Carelli M.D. 1976.Clinch River Breeder Reactor Plant heat transfer correlation for analysis of CRBRP assemblies, Westinghouse, CRBRP-ARD-0034.

[12] Ushakov, P.A., Zhukov, A.V., Matyukhin, N.M., Heat transfer to liquid metals in regular arrays of fuel elements. High Temperature 15 (1977) 868–873, translated from Teplofizika Vysokikh Temperatur, Vol. 15, No. 5, 1977, pp. 1027–1033.

[13] Mikityuk, K., Heat transfer to liquid metal: Review of data and correlation for tube bundles, Nucl. Eng. Des. 239 (2009) 680-687.